J. Fluid Mech. (1992), *vol.* 235, *pp.* 511–528
Printed in Great Britain

Effect of travelling waves on the growth of a plane turbulent wake

By B. MARASLI[1], F. H. CHAMPAGNE[2] AND I. WYGNANSKI[2]

[1] Department of Mechanical Engineering, University of Maryland, College Park, MD 20742, USA

[2] Department of Aerospace and Mechanical Engineering, University of Arizona, Tucson, AZ 85721, USA

(Received 18 January 1991 and in revised form 15 June 1991)

The results of experimental studies on the nonlinear evolution of perturbation waves in the turbulent wake behind a flat plate are presented. Sinuous perturbations at several amplitudes and frequencies were introduced into the wake by oscillating a small trailing-edge flap. The Strouhal numbers of the perturbations were specially chosen so that the downstream location of the neutral point (where the spatial amplification rate obtained from linear theory vanishes) was well within the range of measurements. The streamwise evolution of the waves and their effect on the growth of the turbulent wake was investigated. The amplitude of the coherent Reynolds stress varied significantly with x and changed sign downstream of the neutral point. This resulted in rather strong changes in the spreading rate of the mean flow with x. At high forcing levels, dramatic deviations from the square-root behaviour of the unforced wake occurred. Although the development of the mean flow depended strongly on the forcing level, there were some common features in the overall response, which are discussed. The measured coherent Reynolds stress changed sign in the neighbourhood of the neutral point as predicted by linear theory. The normalized mean velocity profiles changed shape as a result of nonlinear interactions but relaxed to a new self-similar shape far downstream from the neutral point. Detailed measurements of the turbulent and coherent Reynolds stresses are presented and the latter are compared to linear stability theory predictions.

1. Introduction

Large-scale organized structures have been observed in many turbulent free shear flows including the axisymmetric turbulent jet (Crow & Champagne 1971), the two-dimensional mixing layer (Brown & Roshko 1974) and the two-dimensional wake (Grant 1958; Taneda 1959; Castro 1971; Cimbala, Nagib & Roshko 1988). These large-scale coherent structures, which appear to play an important role in the dynamics/evolution of a flow, may result from an instability of the velocity profile to travelling wave disturbances (Gaster, Kit & Wygnanski 1985; Wygnanski, Champagne & Marasli 1986). External forcing of shear flows is often carried out with the intention to enhance, excite or trigger coherent structures and to establish a phase reference. Gaster *et al.* and Wygnanski *et al.* demonstrated the persistence of the coherent structures within forced mixing layers and wakes, respectively, for large streamwise distances (see also Marasli, Champagne & Wygnanski 1991). They applied linear stability theory which incorporated the slow divergence of the mean

flow (Bouthier 1972; Crighton & Gaster 1976) to describe the evolution of the externally introduced coherent structures.

There appears to be a fine line between enhancing already existing structures and introducing something that would not have occurred naturally. Often, when the introduced perturbation is large enough to be detected and be used as a phase reference, it is also large enough to violate the assumptions of linear theory. The nonlinear nature of the problem is evident as the distortion of the mean flow is observed when the wave amplitude is large (Oster & Wygnanski 1982; Weisbrot & Wygnanski 1988). Marasli (1989) and Marasli & Cohen (1989) predicted the local mean flow distortion and the first harmonic (which is generated by the interaction of the fundamental wave with itself) in a wake with a parallel, weakly nonlinear theory. Other dramatic effects of the presence of one or more waves on the mean flow can be found in Strange (1981) and Cohen & Wygnanski (1987), who performed experiments in axisymmetric jets and made comparisons with stability theory which included weakly nonlinear effects. They were able to generate mean flows with non-circular constant-velocity contours by introducing perturbations in two azimuthal modes.

Ko, Kubota & Lees (1970) pointed to the importance of the interaction between the disturbance wave and the mean flow via Reynolds stresses. Coherent Reynolds stress ($-\overline{\tilde{u}\tilde{v}}$) measurements in the two-dimensional mixing layer by Weisbrot & Wygnanski (1988) have revealed some very interesting aspects of this interaction, namely the $-\overline{\tilde{u}\tilde{v}}$ product was observed to change sign at some downstream location, which indicates the reversal of the direction of energy transfer between the mean flow and the perturbation. Cohen (1986) explained the sign reversal by considering a disturbance crossing its neutral point of stability.

Marasli *et al.* (1991) studied the evolution of sinuous perturbation waves in the turbulent wake of a flat plate. The Strouhal number of the perturbations were chosen so that the waves remained amplified over the entire range of measurements. Detailed comparisons between linear stability theory and phase-averaged measurements of the coherent velocity fluctuations show that before significant amplification of the perturbation amplitude occurs, the agreement between the linear theory and the measurements is good. The measured amplitude and phase distributions of the streamwise and lateral components of the coherent or wave-induced velocity fluctuations as well as the coherent Reynolds stress agree well with their counterparts from linear theory. The coherent Reynolds stress, which becomes significant as the perturbation amplitude becomes large, augments the turbulent Reynolds stress causing the spreading rate of the wake to increase. This nonlinear interaction between the fundamental and the mean flow is not strong enough to distort the self-similar shape of the mean velocity profile over the entire range of the measurements. The linear theory predictions deteriorate with increasing downstream distance because of nonlinearity and stronger interaction with the turbulence as the neutral point of the perturbation is approached. Linear stability theory for a slowly diverging flow was used to predict the overall spatial amplification of the perturbation. An eddy-viscosity model was incorporated into the Orr–Sommerfeld equation in an attempt to approximate the effects of turbulence on the evolution of the perturbation. Results from this model show better agreement with the measured data than those from the inviscid calculations. For the unforced flow, the peak in the measured spectrum of the cross-stream velocity fluctuations at any downstream location corresponds to the local neutral frequency predicted by the linear stability theory for inviscid, parallel flow. This result along with the evidence provided by

Wygnanski *et al.* (1986) suggests a possible link between the large-scale coherent structures observed in turbulent wake flows and stability theory.

The objective of the present work is to investigate the effects of spatially travelling sinuous waves on the growth of a two-dimensional, turbulent far wake where the velocity defects are less than 10 % of the free-stream velocity. The Strouhal numbers of the perturbation waves are specially chosen so that the downstream location of the neutral point (where the spatial amplification rate obtained from linear stability theory vanishes) lies within the range of measurements. Various forcing amplitudes are studied, including some large-amplitude cases where strong nonlinear effects are present. When we initiated the present study, the most distinguishing effect of external excitations was an increase in the spreading rate of the wake. The rather dramatic effects on the flow development (similar to those cited for jets and mixing layers) to be presented here have not been observed before for wakes. We attempt to determine the applicability of linear stability theory to describe the experimental results. It will be demonstrated that the linear theory is only able to describe the early stages of the evolution of the structures where the nonlinear effects are less significant.

2. Description of experiments

The experiments were performed at the University of Arizona low-speed wind tunnel facility. The test section of the tunnel is 61 cm wide, 91 cm high, and 6 m long. The flow speed for the present data was in the range 7–10 m/s, corresponding to Reynolds numbers based on the momentum thickness, $Re_\theta \approx 1000$–1400. The flat-plate wake generator was mounted horizontally across the 61 cm span of the test section at a streamwise location 60 cm downstream of the inlet. Measurements of the velocity profile at this plane indicated that the flow was uniform to $\pm 0.25\,\%$. The free-stream disturbance level in the streamwise velocity component was approximately 0.03 %. More details about the facility can be found in Wygnanski *et al.* (1986).

Velocities were measured using a rake of five Dantec 55P51 $\times$-probes connected to Dantec 55M01 and 56C01 constant-temperature anemometers. The total height of the rake was 5.4 cm. The rake was mounted on an internal traversing mechanism with a thin, forward-swept probe support, placing the sensors upstream of any regions of flow interference caused by the mechanism. A Masscomp-5500 with a 16-channel A/D converter and a vector accelerator was used for data acquisition and processing.

For calibration, the hot wires were placed in the free stream, well outside the wake. The conditioned bridge signals and the output of the pressure transducer connected to the Pitot tube were sent to the A/D converter. The $\times$-wires were calibrated against both velocity and yaw angle variations using the procedure described in Wygnanski *et al.* (1986) and Marasli (1989).

The flat-plate wake generator used in the experiments was a solid aluminium plate 30 cm long, 61 cm wide, and 0.635 cm thick. The leading edge of the plate was rounded, and the trailing edge was tapered to 1 mm thickness over the last 10 cm of the chord. Trip wires were placed 3 cm from the leading edge, generating a turbulent boundary layer before the tapered section was reached. Sinuous waves were generated by oscillating a steel flap (0.1 mm thick, 6 mm in chord-length) which was hinged to the trailing edge of the plate with scotch tape. Nylon ribbons were used to connect the downstream edge of both sides of each flap to matched loudspeakers,

which were located on each side of the plate just outside of the tunnel sidewalls. The maximum displacement of the trailing edge of the flap was less than 2 mm (peak-to-peak) for all the cases presented here, except for the very high-amplitude case where it was approximately 4 mm.

3. Results and discussion

3.1. *Constant-frequency forcing at various amplitudes*

Based on the observations of Oster & Wygnanski (1982) and Cohen (1986) in two-dimensional mixing layers, one expects rather pronounced effects in the behaviour of the mean flow as the introduced perturbation goes through the neutral point of amplification. As our objective was to investigate a disturbance that reached its neutral point within the domain of measurements, an appropriate excitation frequency had to be chosen. Marasli *et al.* (1991) computed the amplification rates for sinuous waves of various frequencies using inviscid, linear stability theory and measured mean velocity profiles. It was estimated that a 70 Hz wave should become neutrally stable near $\bar{x} = x/2\theta = 430$. Frequencies in the range from 70 to 100 Hz were chosen for the present experiments.

A range of flap amplitudes was investigated for a frequency of 70 Hz and a free-stream velocity of 7 m/s. The resulting momentum thickness, θ, was 2.2 mm. Forcing levels are given in terms of the response of the flow, $(|\tilde{u}|/u_0)_{\max}$, at a reference location $\bar{x} = 60$, rather than the flap amplitude itself (see the Appendix for brief review of the triple decomposition (Reynolds & Hussain 1972) nomenclature). The streamwise variation of the half-width of the wake L_0 and the centreline velocity deficit u_0(see figure 1) are used to characterize the development of the mean velocity field.

For the unforced wake, the flow is approximately self-preserving with $L_0 \sim x^{\frac{1}{2}}$ and $u_0 \sim x^{-\frac{1}{2}}$, therefore the dimensionless quantity $L_0 U_\infty/\theta u_0$ increases linearly with x. This parameter, which is inversely proportional to the maximum of the mean vorticity at a given x-station of the wake, may be thought of as representing the diffusion of vorticity in the streamwise direction. It is thus an important parameter characterizing the mean motion in the wake and we shall refer to it as the *growth parameter* for brevity. The variation of $L_0 U_\infty/\theta u_0$ with $\bar{x}$ is shown in figure 2 for a variety of forcing levels in the range 0–89 %. The unforced case (hexagons) shows the expected linear growth with $\bar{x}$ while the behaviour of the forced wake depends on the forcing level. It should be noted that the streamwise variation of the individual parameters L_0^2 and $1/u_0^2$ is similar to that of the non-dimensional growth parameter. For the 17 % forcing level the rate of growth of the wake is initially larger than that for the unforced case and the growth parameter diverges almost linearly until $\bar{x} = 300$, after which a break in the slope occurs and the wake stops growing. The wake appears to resume growing further downstream. This type of downstream evolution has not been previously observed for turbulent, two-dimensional wakes. Similar behaviour in the growth of a forced, turbulent, two-dimensional mixing layer was observed by Oster & Wygnanski (1982). When the forcing level is increased to 30 %, the wake develops in a similar manner but the initial growth rate is larger, leading to an earlier, better defined break, followed by a longer region of almost parallel flow. Beyond $\bar{x} = 600$ the wake appears to be growing again ever so slightly. The most striking effect in the development of the growth parameter occurs at the 89 % forcing level. In this case the initial growth is so rapid that it is hardly detected, owing to the relatively large streamwise interval in the measurement. A region of strong

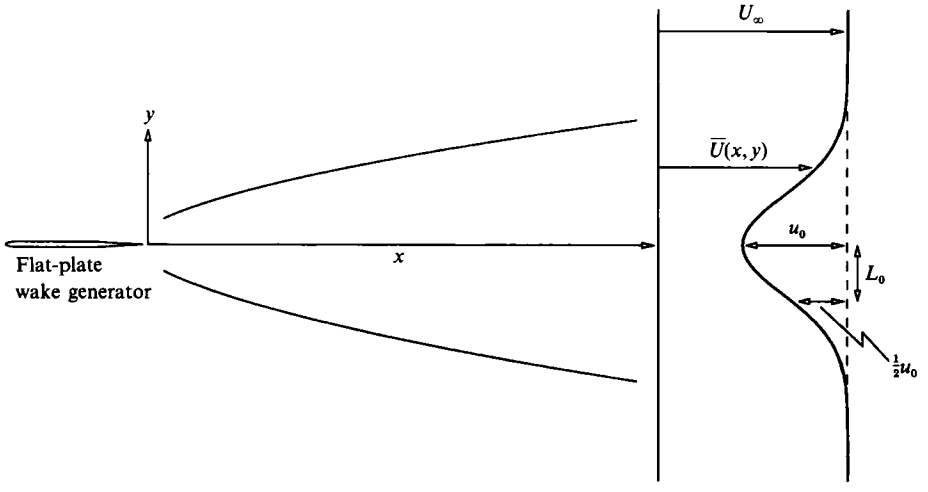

FIGURE 1. A sketch of the wake defining the nomenclature.

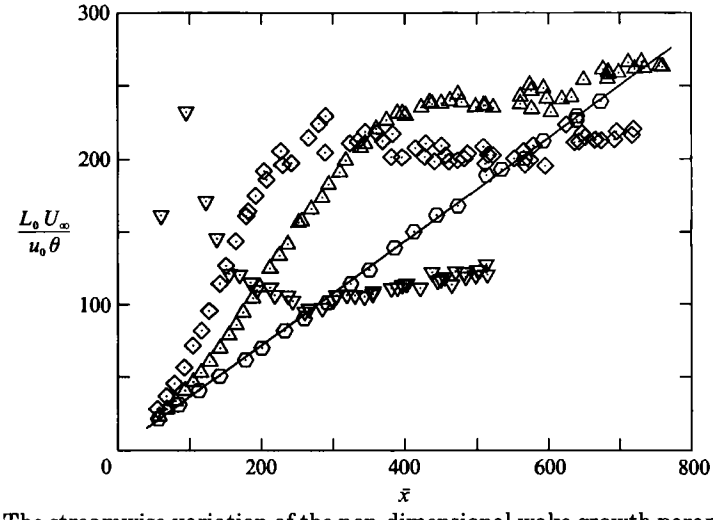

FIGURE 2. The streamwise variation of the non-dimensional wake growth parameter for wakes with various forcing amplitudes and constant forcing frequency (70 Hz): ⊙, unforced; △, low amplitude (17%); ◇, medium amplitude (30%); ▽, high amplitude (89%).

contraction immediately follows the initial region of large growth, and further downstream the wake resumes growing but at a rate that is much less than that of the unforced wake. No parallel-flow region is apparent for this case. The resumption of growth occurs downstream of the location where the growth parameter for the forced wake crosses that of the unforced wake. One should note that, even at the highest forcing level, the coherent structures do not dominate the flow, such as in the wake of an oscillating airfoil reported by Koochesfahani (1989) where at much higher forcing levels the wake flow may exhibit the characteristics of a jet. In the present case the coherent and turbulent Reynolds stresses are of the same order of magnitude, hence a reasonable competition exists between the coherent structures and incoherent turbulence.

The downstream variation in the spreading rate of the mean flow can be better understood by considering the time-averaged x-momentum equation for the small-deficit wake, which in the presence of coherent and turbulent motion takes the form

$$U_\infty \frac{\partial \bar{U}}{\partial x} = -\frac{\partial}{\partial y}(\overline{u'v'} + \overline{\tilde{u}\tilde{v}}). \tag{1}$$

The turbulent Reynolds stress $-\overline{u'v'}$, which dictates the spreading rate of the unforced flow, is augmented by the coherent Reynolds stress $-\overline{\tilde{u}\tilde{v}}$, causing a change in the divergence of the forced wake. As the amplification rate of the perturbation wave changes with x, the amplitude of the coherent stress varies significantly with downstream distance. This results in rather strong changes in the spreading rate of the mean flow with x. Although the development of the mean flow depends strongly on the forcing level, there are some common features in the overall response which can be characterized by three distinct regions. Initially, the rate of growth is nearly linear with x with a slope that is monotonically increasing with the forcing level. Then a break in the slope occurs at $L_0 U_\infty/\theta u_0 \approx 230$, which corresponds to $fL_0/U_\infty \approx 0.22$. We shall refer to the region up to the break point as region I. This value for the non-dimensional frequency near the break point is close to the neutral Strouhal number (St_N) obtained from linear stability calculations using the measured mean velocity profiles. For the inviscid case $St_N = 0.25$, while a value of 0.19 is obtained using a constant eddy-viscosity model ($Re_\theta = 31$) with the Orr–Sommerfeld equation (Marasli, Champagne & Wygnanski 1989, 1991). The exact location of the neutral point is difficult to determine theoretically, as nonlinear terms are not negligible near the end of the amplified region of the disturbance. After the break point, the mean flow readjusts towards the unforced state. The nature of this readjustment depends on the extent of the initial departure from the unforced case and may consist of a gradual growth, an almost parallel behaviour or a contraction. In all cases the mean flow starts spreading again after the growth parameter crosses the unforced line, but the rate of growth is lower than that of the unforced case. The latter behaviour is less obvious for the lower-amplitude cases, although evidence obtained from other data to be subsequently presented supports this claim. We designate the readjustment zone from the break point to the point of intersection with the unforced wake as region II. Downstream of the intersection point will be referred to as region III.

3.2. *Constant-amplitude forcing at various frequencies*

In order to determine the effects of variation in the excitation frequency on the development of the mean flow, data were acquired at several frequencies, holding the initial amplitude of the perturbation constant. Results from two different forcing levels are presented.

Figure 3 displays the variation of the mean flow with streamwise distance for four different excitation frequencies in the range 70–100 Hz, with an approximately constant forcing level of 30%, and $U_\infty = 7$ m/s. The unforced case is again included for comparison. Since the forcing level is defined via the response of the flow rather than the magnitude of an input quantity, adjustment of the amplitude involved an iterative process and the actual forcing levels were 30%, 31%, 33% and 36% for the 70, 80, 90 and 100 Hz data, respectively. The three regions discussed in the previous section are clearly visible. In each case the wake resumes its growth near the point of intersection with the unforced wake. This rate of growth appears to be slower at the lower frequencies of forcing.

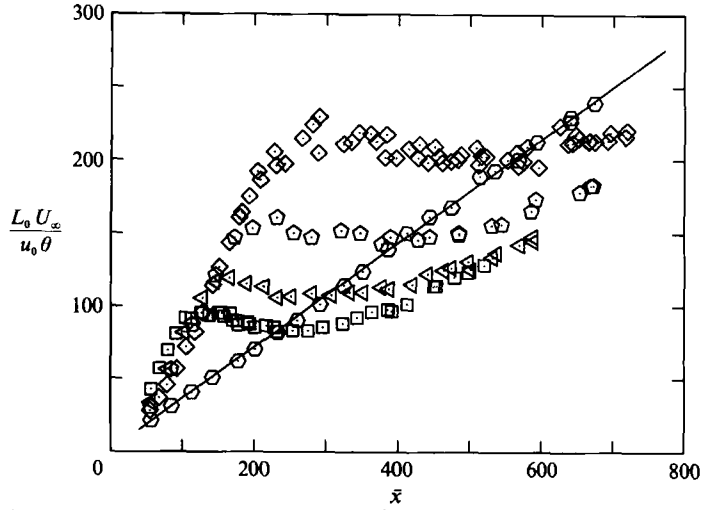

FIGURE 3. The streamwise variation of the non-dimensional wake growth parameter for wakes with various forcing frequencies and constant forcing level (~30%): ⊙, unforced; ◇, 70 Hz; ⊙, 80 Hz; ◁, 90 Hz; ⊡, 100 Hz.

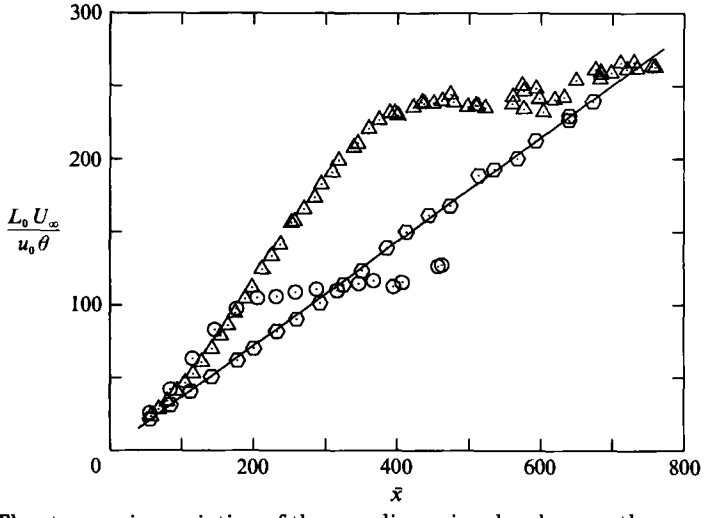

FIGURE 4. The streamwise variation of the non-dimensional wake growth parameter for wakes with various forcing frequencies and constant forcing level (~17%): ⊙, unforced; △, 70 Hz; ⊙, 100 Hz.

Another data set at a lower initial amplitude is presented in figure 4. The forcing level was 17.4% for the 70 Hz data and 19% for the 100 Hz case, forcing an approximately constant-amplitude set. It is quite clear from both figures that the break in the growth occurs earlier and at a lower level as the forcing frequency is increased. On the other hand, the overall shape of the streamwise variation of the growth parameter does not seem to be a function of the excitation frequency. This suggests that groups of data with constant forcing levels could be collapsed on one curve by a suitable non-dimensionalization. This indeed proved to be the case. By inspection of figures 2–4, one sees that both the abscissa and ordinate must be scaled by the frequency. There are several equivalent choices for the scaling. One such choice results in a plot of the local Strouhal number fL_0/U_∞ versus fx/U_∞. The

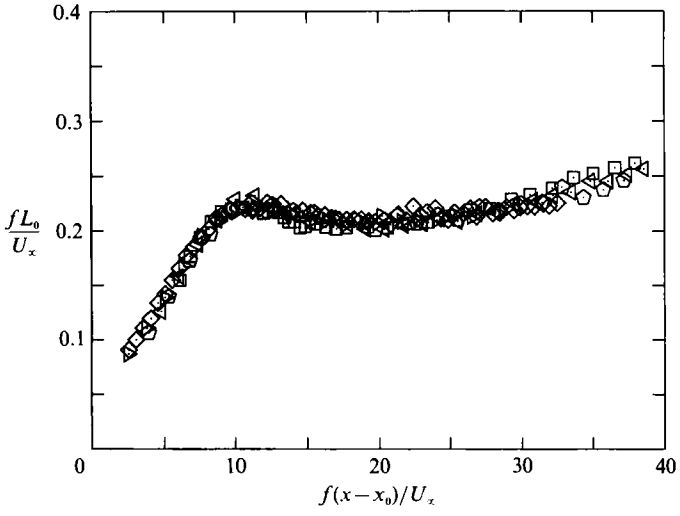

FIGURE 5. The variation of the local Strouhal number versus the scaled streamwise coordinate; ~30% forcing level: ◇, 70 Hz; ⬠, 80 Hz; ◁, 90 Hz; □, 100 Hz; ▷, 100 Hz (10 m/s).

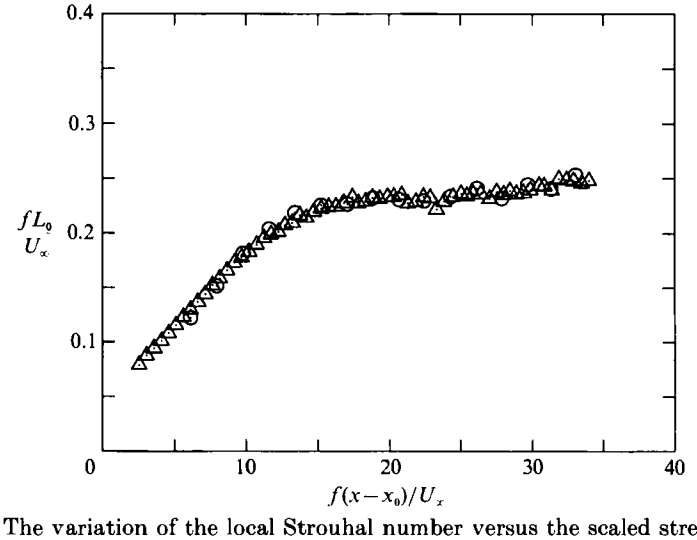

FIGURE 6. The variation of the local Strouhal number versus the scaled streamwise coordinate; ~17% forcing level: △, 70 Hz; ⊙, 100 Hz.

abscissa is the ratio of the streamwise coordinate to the wavelength of the perturbation where the latter remains approximately constant for a slowly diverging, small-deficit wake. The ordinate represents the ratio between the local width of the flow and the wavelength. Figure 5 depicts the ~30% forcing level data (including a set at $U_\infty = 10$ m/s, $f = 100$ Hz), plotted in this manner. A similar plot of the ~17% data is given in figure 6. In both cases, data with different frequencies have collapsed on one curve that is dependent on the forcing level. The Strouhal number at the break point is approximately 0.22 and is associated with the perturbation going through its neutral point.

Since $u_0 L_0/U_\infty \theta = \text{const}$ for small-deficit wakes, replacing the ordinate with $f\theta/u_0$ would have given a similar collapse. The latter quantity is formally identical to the scaling used in the case of a plane mixing layer (Cohen 1986) where θ varies with x

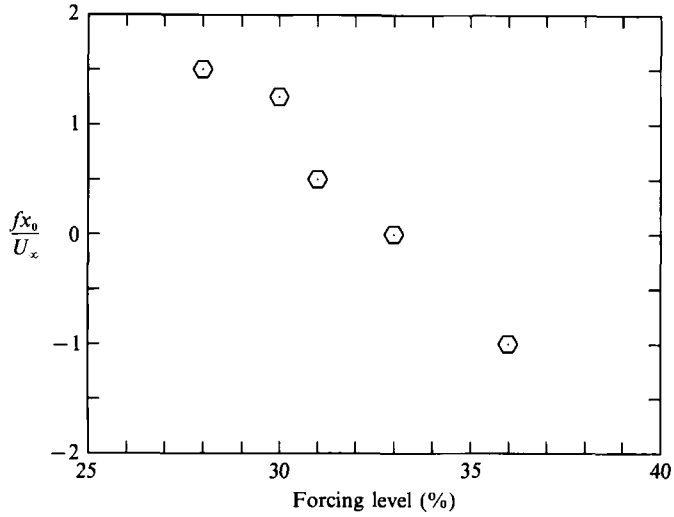

FIGURE 7. The variation of the non-dimensional virtual origin with the forcing level.

while u_0 (average of the two streams) is a constant. In the case of a constant-velocity-ratio mixing layer, the abscissa is identical to the one used in the present case and consequently the analogy between the parameters scaling both flows is complete. The two quantities, fL_0/U_∞ and $f\theta/u_0$, can be combined in the form $f^2(L_0\,\theta/u_0\,U_\infty)$, which would also result in a similar representation.

The virtual origin x_0 in the abscissa provides a translational shift to match the break points of the different data sets. One explanation for the need for a shift can be given by considering the relative amplitudes of the different cases involved. Since the streamwise location of the break point is associated with the neutral point, small variations in the amplitudes among different sets cause the location of the neutral point to shift slightly from one set to the other. Therefore, a small translation of the abscissa is necessary to compensate for the small differences in the forcing levels. The x_0 values used in figure 5 are plotted versus the respective forcing levels in figure 7. Note that, the supposedly constant forcing levels actually vary between 28% and 36%. The 33% data set is arbitrarily assigned a shift of zero. The 36% set, having a larger amplitude, reaches its neutral point earlier than the 33% case, hence requiring a negative offset. Similarly, forcing levels that are less than 33% require positive shifts.

3.3. *Reynolds stress measurements*

Reynolds stress measurements were also obtained for the data presented in the preceding sections. In this section, the development of the total, coherent and turbulent Reynolds stresses are discussed using the 100 Hz, 36% forcing level data as a typical case. The streamwise variation of the growth parameter for the 100 Hz case and the unforced wake is presented in figure 8(*a*). Regions I, II and III are delineated in the plot. The maxima of the Reynolds stress measured at each streamwise location for the positive-y side of the wake are plotted versus $\bar{x}$ in figure 8(*b*). A plot of the Reynolds stresses integrated over the transverse coordinate yields similar information; therefore we shall just present the maxima. In figure 8(*b*) the dashed curve represents the turbulent Reynolds stress $-\overline{u'v'}_{\max}$, the dotted curve corresponds to $-\tilde{u}\tilde{v}_{\max}$ and the dotted-dashed curve represents the total Reynolds stress. The Reynolds stress corresponding to the unforced case is shown with a solid

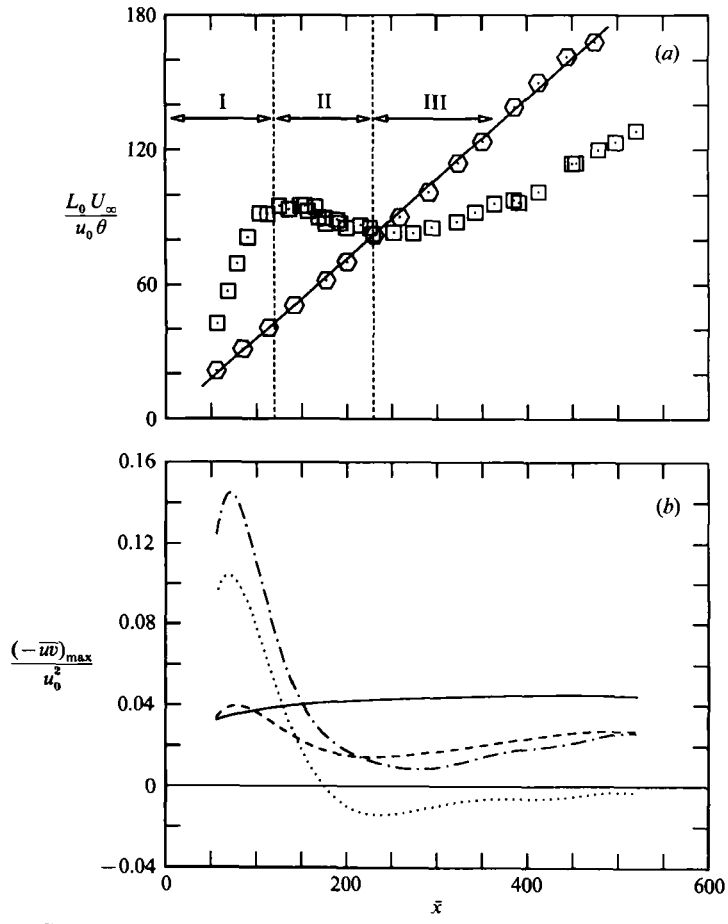

FIGURE 8. Comparison of the streamwise evolution of the growth parameter and the Reynolds stress; 100 Hz, 36% forcing level. (*a*) $L_0 U_\infty/\theta u_0$: ⊙, unforced; ⊡, 100 Hz. (*b*) $(-\overline{uv}/u_0^2)_{max}$: ——, unforced; –·–, total; ....., coherent; – – –, turbulent.

curve. In region I both the turbulent and coherent stresses have the same sign and comparable magnitudes. This results in a larger total Reynolds stress which causes the rapid initial spreading of the mean flow. Note that the break point defining the end of region I does not occur at the downstream location where the coherent stress reverses sign, but it occurs at the location where the coherent and turbulent stresses are of equal magnitude. The x-location where region III begins (corresponding to the intersection of the forced and unforced data on the growth parameter plot) coincides with the location where the turbulent stress overtakes the total stress. In this region the coherent component has reversed its sign and is therefore subtracted from the turbulent component to make the total less than the turbulent part. This is related to the resumption of the growth of the mean flow, but with a smaller slope than that of the unforced case. Further downstream where the coherent component becomes increasingly less important, the total and turbulent parts are almost identical, and the growth parameter curve for the mean wake tends to become parallel to that for the unforced case. Region II is the transitional region between I and III, where the sign reversal of the coherent part occurs.

Transverse distributions of the three Reynolds stress components are plotted for selected streamwise locations in figure 9. In this figure the columns correspond to

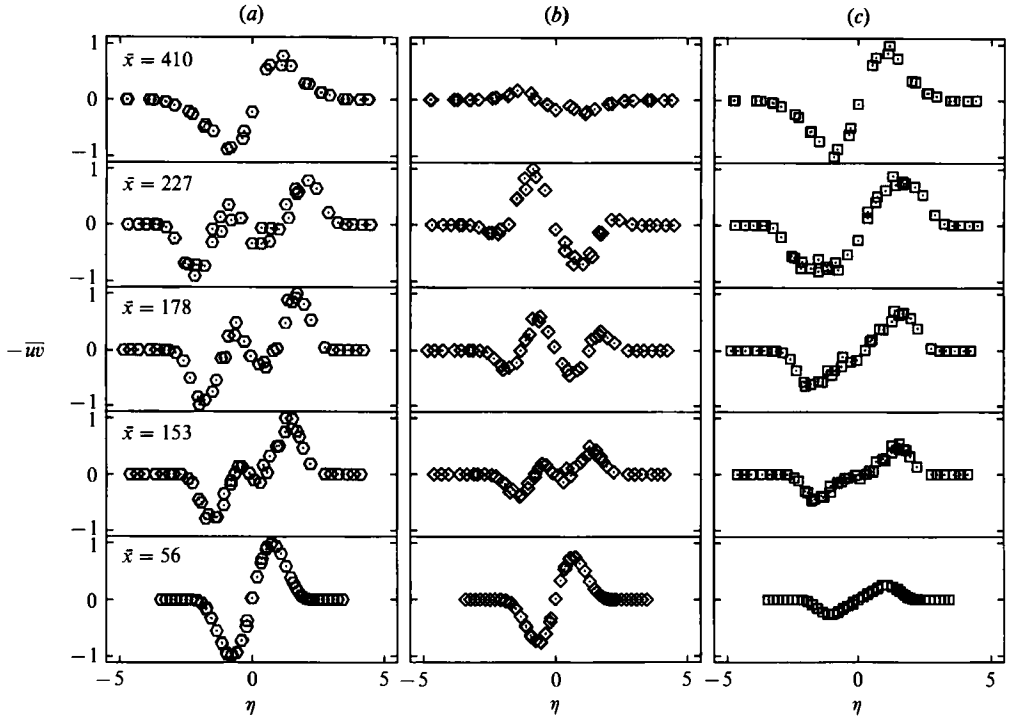

FIGURE 9. The cross-stream Reynolds stress distributions at various x-stations; 100 Hz, 36% forcing level. (*a*) Total (⊙); (*b*) coherent (◇); (*c*) turbulent (⊡).

$-(\overline{u'v'}+\overline{\tilde{u}\tilde{v}})$ (total Reynolds stress), $-\overline{\tilde{u}\tilde{v}}$ (coherent part) and $-\overline{u'v'}$ (turbulent part) respectively. Each row represents a different x-station. The first station is within region I, the next three are in region II and the last one is in region III. The abscissa is the normalized y-coordinate. For each x-station, the ordinates are normalized by the largest of the three to show the relative amount present in each component. Initially, at $\bar{x} = 56$, both the coherent and turbulent parts have similar shapes, with the coherent part constituting $\sim 75\%$ of the total. Data in the second row are taken from the beginning of region II and show a rather peculiar kink which has developed around the centreline of the coherent component. This kink is also apparent in the total Reynolds stress. It is evident from the next rows that this kink is the early stage of a process in which the coherent stress in reversing direction. This transition occurs throughout region II. Finally in region III, the reversal has been completed (fifth row), and the turbulent part has become the dominant component. The turbulent Reynolds stress does not go through a sign reversal. Since the total Reynolds stress is the superposition of the two components, at times it displays rather scattered looking distributions, resulting from the addition of two components with opposing signs (e.g. $\bar{x} = 227$ data in the fourth row). Similar observations were also made in a two-dimensional mixing layer by Weisbrot & Wygnanski (1988).

The sign reversal of the coherent Reynolds stress is related to the fact that the perturbation wave travels through its point of neutral stability (also see Cohen 1986). In order to verify this, the Orr–Sommerfeld equation was solved in the neighbourhood of the neutral point (assuming parallel flow) and the resulting shapes of the Reynolds stress profiles were studied. For demonstration purposes, the parameters from the 100 Hz case were used. In the vicinity of the break point, $u_0 = 0.072$ and the Reynolds number based on the half-width and the molecular

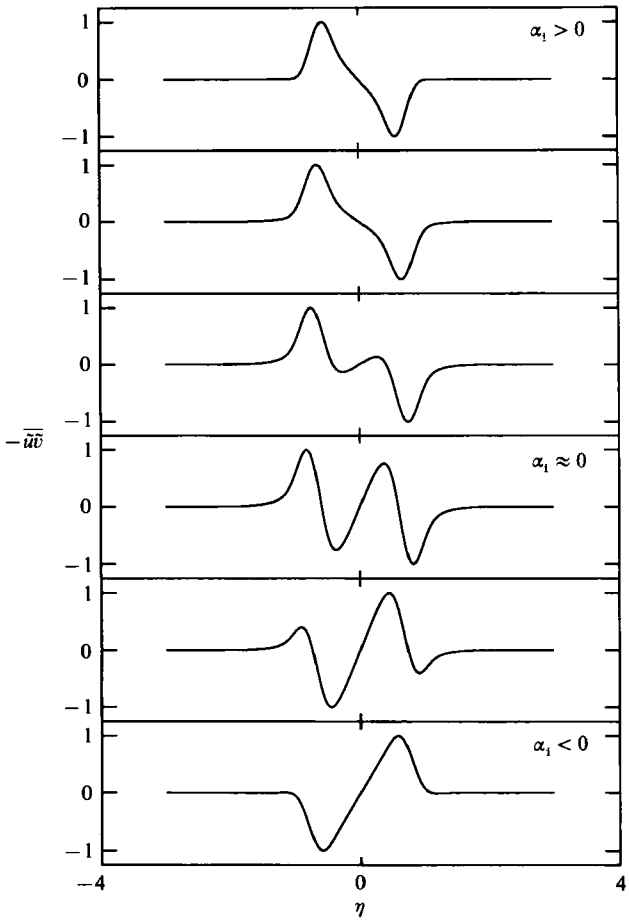

FIGURE 10. The Reynolds stress distributions for a disturbance crossing the neutral point of stability; linear theory.

viscosity is 6300 for the 100 Hz data. The resulting Reynolds stress profiles are plotted in figure 10. As the disturbance passes from the amplified region into the damped region the Reynolds stress profiles change sign and, though the shapes are not identical, the overall transition is quite similar to the experimental measurements presented in figure 9(*b*). For this velocity profile, the linear theory predicts the neutral frequency to be 120 Hz. Hence, according to the linear theory, the 100 Hz wave is still amplified, which does not agree with the conclusions drawn from the Reynolds stress measurements. This overestimation can be attributed to the interaction of the coherent wave with the background turbulence. A similar analysis using a constant eddy-viscosity model ($Re = 210$) gives 72 Hz as the neutral frequency. Near the neutral point, the lengthscales of the most energetic turbulent fluctuations and the wavelength of the excitation are comparable (Marasli *et al.* 1989; Cimbala *et al.* 1988), which may cause the coherent–turbulent field interactions to be too large to be modelled by linear theory.

3.4. *Mean velocity profiles*

The sinuous perturbation waves introduced by the trailing-edge flap are amplified as they propagate downstream. The coherent Reynolds stress eventually can become significant, resulting in the modification of the mean flow. The first sign of nonlinear

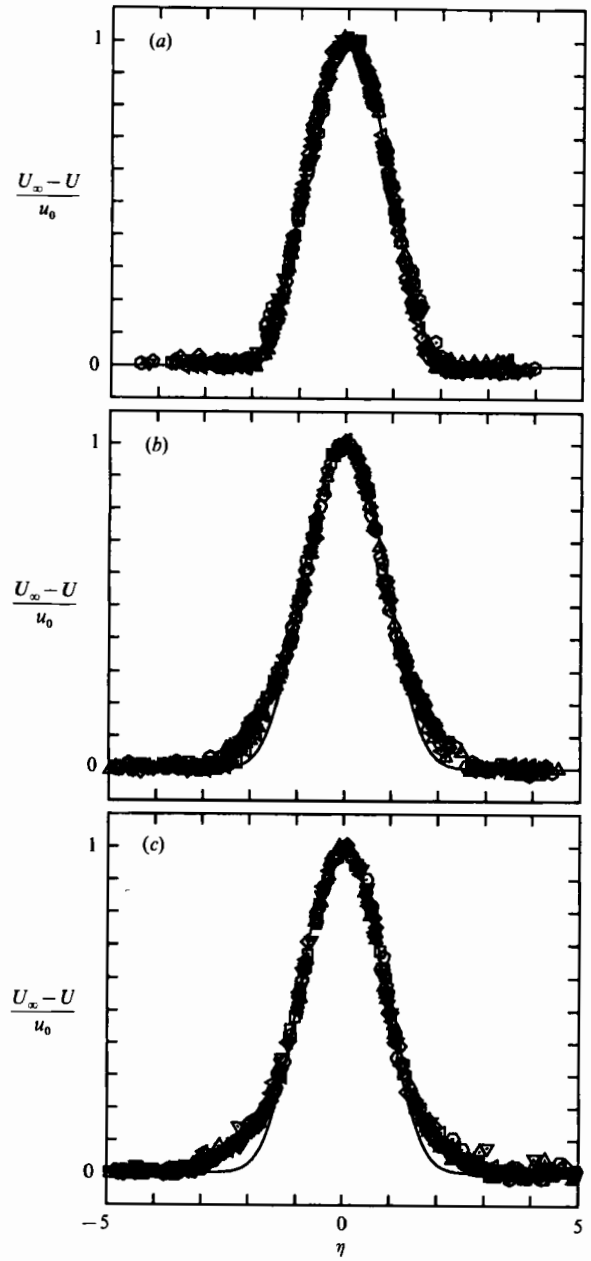

FIGURE 11. The normalized mean velocity profiles at various x-stations and comparison with the unforced profile; 100 Hz, 36% forcing level. (*a*) Region I; (*b*) region II; (*c*) region III. The solid curves represent the unforced profile.

effects on the mean flow is the increased rate of spreading in region I. Here, the coherent Reynolds stress augments the turbulent Reynolds stress causing the spreading rate of the wake to increase. In this initial region, the nonlinear interaction is not strong enough to affect the shape of the mean velocity profile, as can be seen in figure 11(*a*). The profiles plotted are from the 100 Hz data with a 36% forcing level. The abscissa is the non-dimensional transverse coordinate $\eta = y/L_0$. Each symbol represents a different streamwise location. The solid curve is the profile for

the unforced case. The velocity profiles in this region are almost identical to those for the unforced case and are self-similar, even though the forced wake diverges much faster than the unforced wake, as demonstrated in figure 3.

Visible changes in the profiles occur in region II. The profiles in this region for the 100 Hz case are given in figure 11(*b*). Comparison with the solid curve that represents the unforced state indicates that beyond $|\eta| \approx 2$, the forced profiles deviate from the unforced one. Region II is a transitional region where the profiles keep changing and thus are not self-similar.

A different-shaped self-similar velocity profile is found in region III. The difference between this state and that of the unforced case is clearly visible in figure 11(*c*). Similar deviations from the unforced velocity profiles were also observed in a two-dimensional mixing layer by Oster & Wygnanski (1982) and Weisbrot & Wygnanski (1988).

The changes in profile shape can easily be explained by considering (1) with a mean flow given by

$$\bar{U}(x, y) = U_\infty - u_0(x)\, h(\eta), \tag{2}$$

where $h(\eta)$ is the self-similar velocity profile. By substituting (2) into (1) and integrating, one obtains

$$-\frac{\overline{u'v'} + \overline{\tilde{u}\tilde{v}}}{u_0^2} = \frac{1}{u_0}\frac{\mathrm{d}L_0}{\mathrm{d}x}\eta h(\eta). \tag{3}$$

Here we have used the fact that the product $u_0 L_0$, which is proportional to the momentum thickness of the wake, is a constant. For a self-preserving wake, $(1/u_0)(\mathrm{d}L_0/\mathrm{d}x)$ is a constant, hence the Reynolds stress is simply proportional to $\eta h(\eta)$ (see also Wygnanski *et al.* 1986). Although the forced wake is not self-preserving by any means, (3) can still be used to describe the trends as the parameters vary. It is clear that the shape of the mean velocity profile is directly related to the shape of the total Reynolds stress profile. When the latter changes in region II, the former has to change, as seen in figure 11(*b*). Similarly, in regions I and III, where the total Reynolds stress profile conserves its shape, $h(\eta)$ stays invariant (figure 11*a*, *c*). We can also see from (3) that in regions I and III, since $h(\eta)$ does not change, an increase in the left-hand side will increase $(1/u_0)(\mathrm{d}L_0/\mathrm{d}x)$, which translates to an increase in the rate of spreading.

It is interesting that, although far downstream $-\overline{\tilde{u}\tilde{v}}$ is only a small fraction of the total Reynolds stress (see figure 8*b*), within the range of the measurements a return to the original self-similar shape is not observed. It is possible that further downstream, after the coherent disturbance has completely disappeared, the velocity profile will return to its original (unforced) shape; however, the present data do not show any trend in that regard.

3.5. *Comparison with linear stability theory*

Marasli *et al.* (1991) presented detailed comparisons between linear stability theory and phase-averaged measurements of the coherent velocity fluctuations in the turbulent wake of a flat plate with 15% forcing level. The theory, which incorporated the slow divergence of the mean flow, predicted the streamwise evolution of the disturbances quite well. The prediction deteriorated far downstream as the perturbation amplitude reached high enough levels which violated the assumptions for the linear theory.

Since for the cases presented in this article the spatial evolution of the perturbation is a nonlinear process, one cannot expect the linear theory to accurately predict the

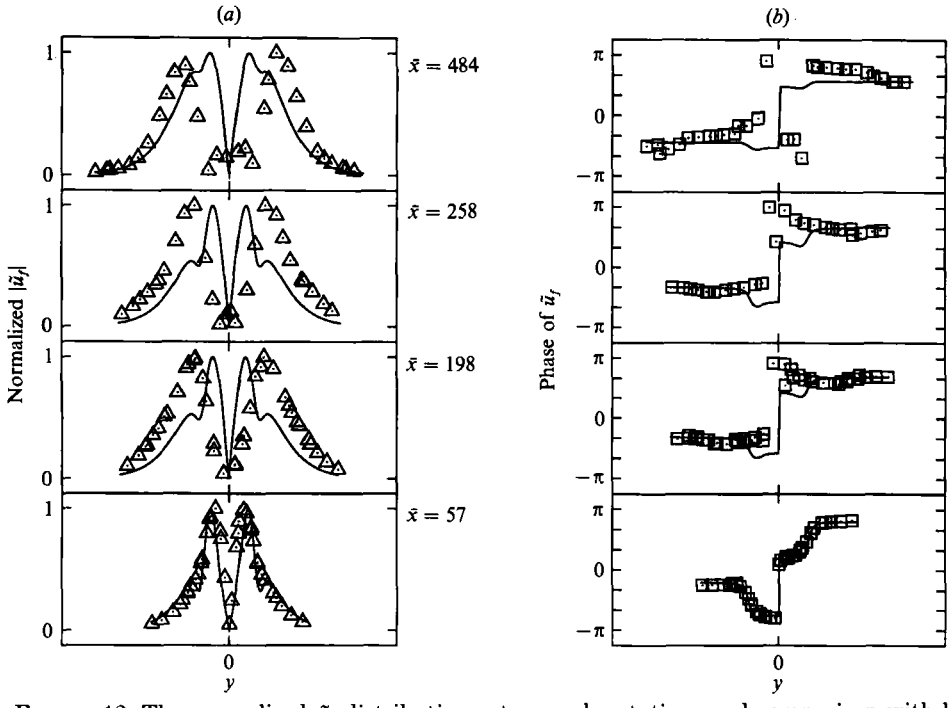

FIGURE 12. The normalized $\tilde{u}_f$ distributions at several x-stations and comparison with linear theory (——); 100 Hz, 36% forcing level. (*a*) Amplitude; (*b*) phase.

experimental results. However, for comparison purposes, we will present mode shapes computed from spatial stability for locally parallel flow and demonstrate the limitations of linear theory. As the linear theory prediction is the first term in the perturbation expansion of a weakly nonlinear theory, at least in the early stages some agreement is expected. The 100 Hz, 36% forcing level data will be used for this purpose.

Figure 12 depicts the $\tilde{u}_f$ amplitudes and phases from several x-stations. The first station is in region I, the second station is in region II and the last one is in region III. The solid lines represent the stability calculations and the symbols correspond to the measurements. (For the details of the stability calculations, the reader is referred to Marasli *et al.* 1989, 1991.) The abscissa is the dimensional y-coordinate. The ordinates in figure 12(*a*) are the normalized amplitudes of $\tilde{u}_f$. Maxima of the measured data and the calculations are matched at each station to compare the local shapes. Relative phase distributions are presented in figure 12(*b*). Since damped modes were anticipated for regions II and III, the molecular viscosity was used in the Orr–Sommerfeld equation. In the amplified region the inviscid calculations are almost identical to those with the molecular viscosity (Marasli *et al.* 1989). In region I, the agreement is very good. However, in regions II and III there are significant differences. The location of the maximum amplitude is not predicted. The computed phase distributions are typical of those for amplified waves, namely the phase difference between the central and outer regions of the wake is negative. However, the measurements indicate a positive phase difference, which is the case for damped waves at high *Re*.

One should note that the failure of the linear theory is not due to the divergence of the wake but to the nonlinearities near the neutral point. This is evident from

figure 8(*a*) where for $100 < \bar{x} < 200$ the flow is almost parallel but the linear theory fails. It is important to note that although the extra divergence of the mean flow occurs owing to the nonlinear growth of the disturbances, part of this nonlinearity can be handled with a linear theory by assuming that the distorted mean flow is known from the experiments, as done by Gaster *et al.*, Wygnanski *et al.* and Marasli *et al.* (1991). However, as displayed here, the part that cannot be handled by the linear theory is when the disturbance approaches the neutral point.

In earlier discussion, the break point in the mean flow was related to the neutral point of stability. However, no statement was made about the exact location of the neutral point; rather it was deduced from the sign reversal of the coherent Reynolds stress. The theory predicts small but positive growth rates at the break point and further downstream. A constant-eddy-viscosity model did not provide a more accurate prediction of the neutral point either. The interaction between the coherent and turbulent fields could be the source of this problem. In general, whenever the excitation frequency is large (say, larger than the local most amplified frequency), the lengthscales of the most energetic turbulent fluctuations and the wavelength of the excitation are comparable, and nonlinear interaction could conceivably be more intense, leading to the failure of linear theory to predict the mode shapes and the amplification rates. Another reason for the failure of linear theory could be the strong critical-layer nonlinearities present near the neutral point, in which case a composite expansion that accounts for both the slow divergence of the wake and nonlinear critical-layer effects as done by Goldstein & Leib (1988) and Goldstein & Hultgren (1988) would be necessary.

4. Conclusions

The nonlinear development of perturbation waves in the turbulent wake of a flat plate was investigated experimentally. As the Strouhal numbers of the perturbations were specially chosen so that the downstream location of the neutral point was well within the range of of measurements, rather interesting effects on the growth of the mean wake flow were observed. The downstream variation in the growth rate of the mean flow is related to the transverse gradient of the total Reynolds stress through the time-averaged x-momentum equation for the small-deficit wake. The turbulent Reynolds stress, which dictates the spreading rate of the unforced flow, is augmented by the coherent Reynolds stress, causing a change in the divergence of the forced wake. The amplitude of the coherent stress varies significantly with downstream distance eventually changing sign in the neighbourhood of the neutral point.

The development of the mean flow depends strongly on the forcing level, but there are some common features in the overall response which can be characterized by three distinct regions. In region I the growth parameter, $L_0 U_\infty/\theta u_0$, varies almost linearly with x and has a slope that is proportional to the forcing level. As both the turbulent and coherent streses have the same sign and comparable magnitudes in this region, this results in a larger total Reynolds stress which causes the rapid initial spreading of the mean flow. A break in the slope occurs where the local Strouhal number, fL_0/U_∞, is approximately 0.22. This value is close to the theoretical values predicted for the neutral Strouhal number. Linear stability calculations using the measured mean velocity profiles give a value of 0.25 for the inviscid case, while a value of 0.19 is obtained using a constant-eddy viscosity model with the Orr–Sommerfeld equation (Marasli *et al.* 1991). The exact location of the neutral point is difficult to determine theoretically as nonlinear terms are not negligible near

the end of the amplified region. The break point defining the end of region I does not occur at the downstream location where the coherent stress reverses sign, but is at the location where the coherent and turbulent stresses are of equal magnitude. After the break point, the mean flow readjusts towards the unforced state in region II. Depending on the extent of the initial departure from the unforced case this readjustment may consist of gradual growth, almost parallel-flow behaviour or contraction. Region III begins at the x-location where the growth parameter crosses the unforced line and this coincides with the location where the turbulent stress is approximately equal to the negative of the coherent stress. In all cases the mean flow starts spreading again, but the rate of growth is lower than that of the unforced case.

Data sets from various cases with different frequencies but identical initial perturbation amplitudes can be collapsed on one curve by plotting fL_0/U_∞ versus fx/U_∞. The former is the ratio of the local width of the wake to the disturbance wavelength, where the latter is the streamwise coordinate scaled with the wavelength.

The variation in the wake growth rate is caused by the nonlinear interaction of the perturbation wave with the mean flow. This can be discussed in terms of the energetics of the flow as follows. In the region upstream of the neutral point (region I), the perturbations are being amplified and energy is transferred from the mean flow to the perturbation. When the coherent stress changes sign through the neutral point, the direction of energy transfer changes and the mean flow gains at the expense of the perturbation. This demonstrates that the lateral rate of spread of the wake is closely linked with the growth of the perturbation wave; amplification of the wave results in a transfer of energy from the mean flow and an increased mean flow divergence. Further evidence to substantiate this can be obtained by noting that the initial divergence of the wake increases with increasing forcing amplitude. The contraction of the wake may be attributed to the transfer of energy from the perturbation wave to the mean flow in the damped region beyond the neutral point.

The normalized mean velocity profiles changed shape as a result of nonlinear interactions but appear to relax to a new self-similar shape far downstream from the neutral point. Detailed measurements of the turbulent and coherent Reynolds stresses are presented and the latter are compared to linear stability theory predictions. The qualitative features of the sign reversal in the coherent Reynolds stress predicted by the Orr–Sommerfeld solutions are quite similar to those in the measurements. However, linear stability theory failed to predict the evolution of the disturbances except for the early stages where the perturbation amplitudes were low.

The authors are grateful for the financial support provided by the Air Force Office of Scientific Research under contract No. 85-0146. B.M. would like to acknowledge the sponsorship of the University of Maryland Minta Martin Fund during the later stages of the work.

Appendix

In the presence of coherent motion such as the one we have introduced externally, an instantaneous variable (for example, the streamwise velocity) can be considered to consist of three components (Reynolds & Hussain 1972):

$$u(\boldsymbol{x},t) = \bar{U}(\boldsymbol{x}) + \tilde{u}(\boldsymbol{x},t) + u'(\boldsymbol{x},t). \tag{A 1}$$

Here $\bar{U}$ is the mean or time-averaged part, $\tilde{u}$ is the coherent part representing the

periodic wave contribution, and u' represents the incoherent turbulent fluctuations. Here $\tilde{u}$ can be obtained from the phase average, which is defined as

$$\langle u(\boldsymbol{x},t)\rangle = \lim_{N\to\infty}\frac{1}{N}\sum_{n=1}^{N} u(\boldsymbol{x},t+nT) = \bar{U}(\boldsymbol{x})+\tilde{u}(\boldsymbol{x},t), \tag{A 2}$$

where T is the period of the coherent fluctuations.

The total Reynolds stress is defined as the correlation of the total velocity fluctuations in the streamwise and cross-stream directions, and is given by

$$-\overline{(\tilde{u}+u')(\tilde{v}+v')} = -(\overline{\tilde{u}\tilde{v}}+\overline{u'v'}), \tag{A 3}$$

where we have used the fact that the coherent and turbulent velocity fluctuations are uncorrelated.

REFERENCES

Bouthier, M. 1972 *J. Méc.* **11**, 599.

Brown, G. L. & Roshko, A. 1974 *J. Fluid Mech.* **64**, 775.

Castro, I. 1971 *J. Fluid Mech.* **46**, 599.

Cimbala, J. M., Nagib, H. M. & Roshko, A. 1988 *J. Fluid Mech.* **190**, 265.

Cohen, J. 1986 Instabilities in turbulent free shear flows. Ph.D. thesis, University of Arizona.

Cohen, J. & Wygnanski, I. 1987 *J. Fluid Mech.* **176**, 221.

Crighton, D. G. & Gaster, M. 1976 *J. Fluid Mech.* **77**, 397.

Crow, S. C. & Champagne, F. H. 1971 *J. Fluid Mech.* **48**, 547.

Gaster, M., Kit, E. & Wygnanski, I. 1985 *J. Fluid Mech.* **150**, 23.

Goldstein, M. E. & Hultgren, L. S. 1988 *J. Fluid Mech.* **197**, 295.

Goldstein, M. E. & Leib, S. J. 1988 *J. Fluid Mech.* **191**, 481.

Grant, H. L. 1958 *J. Fluid Mech.* **4**, 149.

Ko, D. R. S., Kubota, T. & Lees, L. 1970 *J. Fluid Mech.* **40**, 315.

Koochesfahani, M. M. 1989 *AIAA J.* **27**, 1200.

Marasli, B. 1989 Spatially travelling waves in a two-dimensional turbulent wake. Ph.D. thesis, University of Arizona.

Marasli, B., Champagne, F. H. & Wygnanski, I. 1989 *J. Fluid Mech.* **198**, 255.

Marasli, B., Champagne, F. H. & Wygnanski, I. 1991 *Phys. Fluids* A **3**, 665.

Marasli, B. & Cohen, J. 1989 *Bull. Am. Phys. Soc.* **34**, 2260.

Oster, D. & Wygnanski, I. 1982 *J. Fluid Mech.* **123**, 91.

Reynolds, W. C. & Hussain, A. K. M. F. 1972 *J. Fluid Mech.* **54**, 263.

Strange, P. J. R. 1981 Spinning modes in orderly jet structure and jet noise. Ph.D. thesis, University of Leeds.

Taneda, S. 1959 *J. Phys. Soc. Japan* **14**, 843.

Weisbrot, I. & Wygnanski, I. 1988 *J. Fluid Mech.* **195**, 137.

Wygnanski, I. J., Champagne, F. H. & Marasli, B. 1986 *J. Fluid Mech.* **168**, 31.